TU Delft

Delft University of Technology

Improved catalyst formulations for the conversion of glycerol to bio-based aromatics

He, Songbo; Kramer, Thomas Sjouke; Klein, Frederike Gerda Hiltje; Chandel, Anshu; Tegudeer, Zhuorigebatu; Heeres, Andre; Liu, Chuncheng; Pidko, Evgeny; Heeres, Hero Jan

DOI
10.1016/j.apcata.2021.118393

Publication date
2022

Document Version
Final published version

Published in
Applied Catalysis A: General

Citation (APA)
He, S., Kramer, T. S., Klein, F. G. H., Chandel, A., Tegudeer, Z., Heeres, A., Liu, C., Pidko, E., & Heeres, H. J. (2022). Improved catalyst formulations for the conversion of glycerol to bio-based aromatics. *Applied Catalysis A: General*, *629*, Article 118393. https://doi.org/10.1016/j.apcata.2021.118393

Important note
To cite this publication, please use the final published version (if applicable).
Please check the document version above.

Copyright
Other than for strictly personal use, it is not permitted to download, forward or distribute the text or part of it, without the consent of the author(s) and/or copyright holder(s), unless the work is under an open content license such as Creative Commons.

Takedown policy
Please contact us and provide details if you believe this document breaches copyrights.
We will remove access to the work immediately and investigate your claim.

This work is downloaded from Delft University of Technology.
For technical reasons the number of authors shown on this cover page is limited to a maximum of 10.

Applied Catalysis A, General 629 (2022) 118393

Contents lists available at ScienceDirect

Applied Catalysis A, General

journal homepage: www.elsevier.com/locate/apcata

Improved catalyst formulations for the conversion of glycerol to bio-based aromatics

Songbo He [a], Thomas Sjouke Kramer [a], Frederike Gerda Hiltje Klein [a], Anshu Chandel [a], Zhuorigebatu Tegudeer [a], Andre Heeres [b], Chuncheng Liu [c], Evgeny Pidko [c], Hero Jan Heeres [a,*]

[a] Green Chemical Reaction Engineering, Engineering and Technology Institute Groningen, University of Groningen, Nijenborgh 4, 9747 AG Groningen, The Netherlands
[b] Hanze University of Applied Sciences, Zernikeplein 11, 9747 AS Groningen, The Netherlands
[c] Inorganic Systems Engineering Group, Department of Chemical Engineering, Delft University of Technology, 2629 HZ Delft, The Netherlands

ARTICLE INFO

Keywords:
Catalytic pyrolysis
BTX
Bio-based chemicals
ZSM-5
Binder

ABSTRACT

The catalytic conversion of glycerol to aromatics (GTA, *e.g.*, benzene, toluene, and xylenes, BTX) over a shaped H-ZSM-5/Al_2O_3 (60/40 wt%) catalyst was investigated in a continuous fixed-bed reactor to study the addition of the Al_2O_3 binder in the catalyst formulation on catalyst performance. The experiments were performed under N_2 at 550 °C, a WHSV of glycerol (pure) of 1 h^{-1}, and atmospheric pressure. The spent H-ZSM-5/Al_2O_3 catalysts were reused after an oxidative regeneration at 680 °C and in total 5 reaction-regeneration cycles were performed. Catalyst characterization studies show that the addition of the Al_2O_3 binder does not affect the surface area and crystallinity of the formulation, but increases the total pore volume (mesopores in particular) and total acidity (Lewis acidity in particular). The H-ZSM-5/Al_2O_3 (60/40 wt%) catalyst shows a considerably prolonged catalyst life-time (8.5 *vs.* 6.5 h for H-ZSM-5), resulting in a significant increase in the total BTX productivity (710 *vs.* 556 mg g^{-1} H-ZSM-5). Besides, the addition of the Al_2O_3 binder retards irreversible deactivation. For instance, after 3 regenerations, catalyst performance is comparable to the fresh one. However, after 4 regenerations, some irreversible catalyst deactivation occurs, associated with a reduction in total pore volume, crystallinity, and acidity (Brønsted acidity in particular), and meso-porosity of the Al_2O_3 binder. This study shows that both the stability and reusability of H-ZSM-5-based catalysts for GTA are remarkably enhanced when using a suitable binder.

1. Introduction

Valorization of crude glycerol co-produced in the bio-diesel industry is of high relevance to improve the techno-economic viability of bio-diesel. In the last decades the application of crude [1] or, most commonly, purified glycerol [2] for the production of value-added bio-based chemicals by various catalytic conversion processes has been studied extensively [3]. The *ex-situ* catalytic pyrolysis of crude glycerol to bio-based aromatics is considered an attractive valorization route for crude glycerol and was demonstrated at a pilot-scale unit in 2019 [4]. With this approach, the glycerol is separated from the inorganic impurities in a thermal pyrolysis reactor [5]. The vapor phase, consisting of glycerol, glycerol decomposition products (C_1 - C_3 oxygenates [6]), residual fatty acids, and decomposition products thereof (short- and long-chain hydrocarbons [7]), is subsequently converted in a catalytic upgrading reactor to form aromatics (benzene, toluene, and xylenes (abbreviated as BTX), and higher aromatics). For instance, a BTX yield of *ca.* 14.6 C.% (on a carbon basis) was reported when using an H-ZSM-5/bentonite catalyst in combination with crude glycerol [5].

By far more attention has been given to the use of purified glycerol for aromatics synthesis using zeolite-based catalysts [8]. Among them, MFI-type ZSM-5 zeolites with Lewis and Brønsted acid sites located in the three-dimensional micro-pores [9] show the highest aromatics yield [10]. For instance, a peak carbon yield of BTX of *ca.* 28 C.% and a total BTX productivity of *ca.* 398 mg BTX g^{-1} H-ZSM-5 has been reported recently using H-ZSM-5 catalyst [6]. Significant BTX yield improvements are possible when using metal-promoted H-ZSM-5-based catalysts [11–14]. As an example, the BTX yield was significantly increased (from 9.75 C.% over a pristine H-ZSM-5 to 43.2 C.%) when using a Pd/H-ZSM-5 catalyst in combination with H_2 [11].

A major issue regarding the use of ZSM-5-based catalysts for the conversion of glycerol to aromatics is the limited catalyst lifetime due to coke formation on the catalyst [5,6,10,15–19], Typically, up to 8–15 wt % of coke is present on spent H-ZSM-5-based catalysts [5,6,15,18,19].

* Corresponding author.
E-mail address: h.j.heeres@rug.nl (H.J. Heeres).

https://doi.org/10.1016/j.apcata.2021.118393
Received 3 August 2021; Received in revised form 25 September 2021; Accepted 7 October 2021
Available online 10 October 2021
0926-860X/© 2021 The Authors. Published by Elsevier B.V. This is an open access article under the CC BY license (http://creativecommons.org/licenses/by/4.0/).

Modifications of the zeolite structure by *e.g.* metal incorporation and by using hierarchical structures have been shown to reduce the rate of coke deposition, leading to a prolonged catalyst life-time, *e.g.*, from *ca.* 5.5 h for the pristine H-ZSM-5 [13,17] to *ca.* 10 h for the Sn-modified H-ZSM-5 [13] and *ca.* 19 h for a hierarchical H-ZSM-5 [17]. Alternatively, the introduction of binders to an H-ZSM-5 catalyst has also resulted in extended catalyst life-times, *e.g.*, from *ca.* 220 min for H-ZSM-5 to *ca.* 320 min for H-ZSM-5/Al_2O_3 (90/10 wt%) [19].

Catalyst deactivation by coking is considered reversible as the coke can be removed easily by an oxidative treatment [10,16]. However, typically also irreversible catalyst deactivation occurs after a few reaction-regeneration cycles [5,6,13,16], associated with a reduction of the microporosity, crystallinity, and Lewis and Brønsted acidity of the regenerated catalysts [5,6]. This has a negative impact on catalyst performance and leads for instance to a reduction in peak BTX yield, total BTX productivity, and catalyst lifetime [6,13,14,16,20].

In a recent preliminary screening investigation, we have shown that the addition of binders (alumina, silica, and clays) to H-ZSM-5 has positive effects on catalyst performance and particularly lifetime [19]. We here report an in-depth study on the use of a shaped H-ZSM-5/Al_2O_3 catalyst (granules, ϕ 1.2–1.8 mm, 40 wt% alumina) for the conversion of glycerol to aromatics and compare the performance with those of the individual catalyst components. The fresh catalysts were characterized in detail using various techniques and tested in a continuous set-up for glycerol conversion to aromatics, with a special emphasis on the synergic effects between the H-ZSM-5 and the binder. The regenerability of the shaped H-ZSM-5/Al_2O_3 catalyst was tested by performing 5 reaction-regeneration cycles, followed by detailed characterization of spent catalysts to identify possible deactivation pathways.

2. Experimental

2.1. Materials

An H-ZSM-5 zeolite with a relative low SiO_2/Al_2O_3 molar ratio (28, termed as H-ZSM-5(28)) was applied in this study. This ratio was selected based on an optimization study in the literature [12], showing that the BTX yield over H-ZSM-5 zeolites follows a volcano-shape relationship with the SiO_2/Al_2O_3 ratio (23−280) with a maximum performance for a SiO_2/Al_2O_3 ratio of *ca.* 30. H-ZSM-5(28) powder, boehmite powder, and H-ZSM-5/Al_2O_3 granules (ϕ 1.2–1.8 mm, prepared by using H-ZSM-5 (60 wt%) and γ-Al_2O_3 (40 wt%) powder as the raw materials) were supplied by the Yangzhou Baisheng Catalyst Co., Ltd., PR China. Glycerol (> 99.5% purity, s.g. 1.26) was supplied by Boom BV, The Netherlands. The analytical-grade reagents such as *n*-nonane, ethanal, and tetrahydrofuran, were supplied by Sigma-Aldrich. Ar (liquid) and N_2 (liquid and technical-grade gas) were supplied by Linde.

2.2. Catalysts preparation

Fractions of H-ZSM-5 and Al_2O_3 with specific particle size ranges (0.5–0.8 mm) were prepared using a pelletizing/sieving sequence. For this purpose, the individual feeds (H-ZSM-5 or Boehmite) were pelletized in a die (ϕ 13 mm) using a pellet press (Model 4350, Carver Inc.) at a pressure of *ca.* 1 ton cm^{-2}, followed by crushing using an Agate pestle and mortar set (IDL GmbH & Co. KG) and sieving using stainless steel analytical sieves (Linker Industrie-Technik GmbH). Both these samples and the as-received H-ZSM-5/Al_2O_3 granules were calcined before use. For this purpose, the component was loaded to a Haldenwanger porcelain crucible (supplied by Fisher Scientific Nederlands) at room temperature, followed by gradual heating to 600 °C (1 °C min^{-1}), isothermal calcination at 600 °C for 8 h, and gradual cooling to 25 °C (1 °C min^{-1}) in a LT 9/11/P330 muffle furnace (Nabertherm GmbH). The calcined H-ZSM-5, γ-Al_2O_3, and H-ZSM-5/Al_2O_3 catalysts were stored in a Bel-Art™ F42400–2141 vacuum desiccator (BEL-ART - SP Scienceware & HB Instruments, *ca.* 0.1 bar) filled with silica gel indicating desiccant (supplied by Fisher Scientific Nederlands, product No. 11418580).

2.3. Catalytic conversion of glycerol to aromatics

The catalytic conversion of glycerol to aromatics was performed in a dedicated GTA-10 unit (Fig. S1) equipped with a tubular reactor (stainless-steel tubing, ϕ 1 × 0.083 in., length of 300 mm, supplied by Swagelok with part No. SS-T16-S-083–6ME) and a stainless-steel jacket (ϕ 44 × 9 mm, supplied by Salomon's Metalen BV, The Netherlands). The fresh catalyst (10 g) was sandwiched between quartz wool (supplied by VWR international, part No. BEHRB00027716). The reactor was gradually heated to the reaction temperature of 550 °C (5 °C min^{-1}) and then maintained at this temperature to pretreat the catalyst for *ca.* 2 h (to remove the adsorbed water) under an N_2 flow (50 ml min^{-1}). The as-received glycerol was loaded to two 100-ml gastight syringes (supplied by Hamilton, part No. 86020) and pumped (10 g h^{-1}) by two NE-1010 syringe pumps (supplied by Prosense BV, The Netherlands) into a preheater (300 °C). The mixture of N_2 (50 ml min^{-1}) and the glycerol vapor was first sent to a purge vent (Fig. S1) to purge the lines for *ca.* 2 h (during the pretreatment of the catalyst) and was then switched to the reactor (550 °C).

The reaction was performed at near atmospheric pressure (*viz.*, P2 and P3 were < 3 mbar, Fig. S1), which was indicated by JUMO dTRANS p30 pressure transmitters (supplied by RS Components BV, The Netherlands, part No. 613–7732) coupled with AUF-1000 readers (supplied by Kobold BV, The Netherlands). After the reaction, the vapor products were introduced to the downstream condensation and separation system. There, two parallel condensers and gas-liquid separators were present which were swapped every 30 min to collect the products at a different time on stream (TOS) by automatically switching the three pneumatic valves (*viz.*, V11, V12, and V15, Fig. S1, supplied by Swagelok, part No. AMSTR-SS-43GXS4-A15XD), which were controlled by a Grasslin digital time switch (supplied by RS Components BV, The Netherlands with part No. 388–442).

The experiments were run continuously for a certain TOS until negligible BTX (carbon yield < 1 C.%) was present in the liquid product, which was visually indicated by the formation of a homogeneous liquid product phase (instead of two immiscible liquids) [6] and off-line product analyses (*vide infra*). The H-ZSM-5/Al_2O_3 catalyst was tested twice under similar conditions to check the repeatability of the experiments (Fig. S2).

2.4. Catalyst regeneration and reuse of the H-ZSM-5/Al_2O_3 catalyst for 5 reaction-regeneration cycles

The used catalyst (denoted as used-i, where i indicates the times used in the reactor) was unloaded from the reactor followed by regeneration. The apparatus and protocol for the *ex-situ* catalyst regeneration under air were similar to those for catalyst calcination (*vide supra*), except that a higher temperature of 680 °C and a longer time of 12 h were applied.

The regenerated H-ZSM-5/Al_2O_3 catalyst (denoted as regenerated-i, where i indicates the times regenerated in the oven) was re-loaded to the reactor. A similar protocol as used for testing the fresh catalyst (*vide supra*) was applied to evaluate the performance of the regenerated catalyst. The reaction-regeneration cycle was performed 5 times to determine the regenerability of the H-ZSM-5/Al_2O_3 catalyst.

2.5. Product analyses

Typically, a biphasic liquid system with an organics and aqueous phase was obtained after the reaction. To obtain a homogeneous solution to facilitate analyses, a stock solution consisting of *n*-nonane (*ca.* 20,000 ppm), ethanol (*ca.* 9 vol%), and THF, was added. Quantification of the aromatics was done using an HP 5890 GC-FID and HP 6890/5973 GC-MS, both of which were equipped with an Rtx-1701 column (30 m × 0.25 mm × 0.25 μm, supplied by Restek). The gaseous products were

collected in 5-L FlexFoil Plus gas bags (supplied by SKC Ltd. With part No. 207104,) and directly analyzed on a pre-calibrated HP 5890 GC-TCD equipped with a CP-PoraBOND Q column (50 m × 0.53 mm × 10 μm, supplied by Varian) and an HP-Molesieve column (30 m x 0.53 mm x 50 μm, supplied by Agilent). Catalyst performance such as yields of products (on a carbon basis), individual BTX selectivity, total BTX productivity, and turnover number (TON) were calculated by Eqs. (1)–(4).

$$\text{Carbon } \textit{yield} \text{ of product } (\%) = \frac{\text{mol of } \textit{carbon} \text{ in the individual } \textit{product}}{\text{mol of carbon in glycerol } \textit{feed}} \times 100 \quad (1)$$

$$\text{Individual BTX selectivity } (\%) = \frac{\text{mol of carbon in the individual } \textit{BTX}}{\text{mol of carbon in total BTX } \textit{product}} \times 100 \quad (2)$$

$$\text{Total BTX productivity } \left(\text{mg}_{\text{BTX}}\ \text{g}^{-1}_{\text{catalyst}}\right) = \frac{\text{weight of total BTX produced}}{\text{weight of catalyst}} \quad (3)$$

$$\text{TON } \left(\text{mol}_{\text{BTX}}\ \text{mol}^{-1}_{\text{acid site}}\right) = \frac{\text{total BTX production during } \textit{TOS}}{\text{number of Brønsted acid sites according to Pyridine IR } \textit{analysis}} \quad (4)$$

2.6. Catalyst characterization

High-resolution transmission electron microscopy (HR-TEM) images of the catalyst were taken on a Tecnai T20 electron microscope (FEI) equipped with an X-Max T80 SDD detector (Oxford) for Energy Dispersive X-ray (EDX) analyses. Before analyses, the catalyst was dispersed in ethanol followed by deposition on a holy carbon-coated copper grid (Quantifoil 1.2/1.3). Semi-quantification of the elements (C, Al, and Si) on the catalysts was performed by analyzing the particles in the holes of the grid to avoid interference with the grid.

X-ray fluorescence (XRF) was conducted on an Epsilon 3XLE spectrometer (PANalytical) using the fundamental parameters method. The samples were measured in the form of powders and the elements were determined in the form of oxides.

Physisorption of Ar at 87 K and N_2 at 77 K was carried out on an ASAP 2420 (Micromeritics) to measure Brunauer-Emmett-Teller (BET method) surface area, total pore volume (at P/P_0 of 0.98), Barrett-Joyner-Halenda (BJH method) mesopore size distribution, and micropore size distribution and volume based on Non-Localized Density Functional Theory (NLDFT [21]). The catalysts were degassed at 450 °C for 4 h and the free-space of the sample tubes was also determined before measurements.

Powder X-Ray Diffraction (PXRD) patterns were recorded on a D8 Advance Powder Diffractometer (Bruker) by an LYNXEYE detector (1D mode). Cu Kα radiation (λ = 1.5418 Å) was used and operated at 40 kV and 40 mA. Relative crystallinity of the catalyst was calculated according to the ASTM D5758–01 method shown in Eq. (5), where H represents the height of the peak at 2θ = 24.37°.

$$\text{Relative crystallinity } (\%) = \frac{H_{\text{catalyst}}}{H_{\text{fresh H-ZSM-5}}} \times 100 \quad (5)$$

Temperature programmed desorption of ammonia (NH_3-TPD) was carried out on an AutoChem II (Micromeritics) equipped with a TCD with a calibration curve for NH_3 quantification. The catalyst was first pretreated at 550 °C in He for 1 h, then exposed to an NH_3/He (1.0 vol %) stream at 100 °C for 1 h, and finally purged using He for 1 h. Desorption of ammonia from the catalyst surface was performed by increasing the temperature to 550 °C at a heating rate of 10 °C min^{-1}.

Pyridine-IR spectra were measured on a Nicolet 6700 FTIR spectrometer using a tailor-made cell. The catalysts were vacuumed at 400 °C (< 10^{-3} bar) followed by the adsorption of pyridine vapor at 25 °C. Then, the catalysts with adsorbed pyridine were evacuated at 160 °C before the analyses.

Magic angle spinning solid-state nuclear magnetic resonance (MAS ssNMR) spectra were measured on an AV-I 750 MHz spectrometer (Bruker). A magnetic field of 17.6 Tesla, a MAS rate of 54.74, and a scan number of 1024 were applied. Chemical shifts for ^{27}Al and ^{29}Si MAS ssNMR spectra were referenced to $Al(NO_3)_3$ and tetramethylsilane.

Thermogravimetric analysis (TG) and differential thermogravimetry (DTG) was conducted on a TGA5500 thermogravimetric analyzer (TA Instruments). The temperature was programmed from 25 °C to 800 °C with a ramp rate of 10 °C min^{-1}.

Elemental (CHN) analysis was performed on a EuroEA3000 (Eurovector), using sulfanilamide (Elemental Microanalysis Ltd.) as the standard reference. Analyses were performed at least in duplicate and the average value is reported.

3. Results and discussions

3.1. Catalytic pyrolysis of glycerol to bio-based aromatics

The catalytic pyrolysis of glycerol (> 99.5 purity) to bio-based aromatics was performed continuously in a fixed bed reactor (GTA-10 unit, Fig. S1) using three catalysts: H-ZSM-5 (28)/Al_2O_3, and the two individual components (H-ZSM-5 (28) and Al_2O_3). All experiments were carried out using a shaped catalyst with a particle size range between 1.2 and 1.8 mm, a catalyst loading of 10 g, a catalyst bed temperature of 550 °C, atmospheric pressure, and a glycerol WHSV of 1 h^{-1}. The liquid phase from the reactor (two immiscible liquid phases in case of significant BTX formation, an organic and aqueous one) was collected for a 30 min time interval and analyzed. These conditions are based on optimization experiments using H-ZSM-5/Al_2O_3 and are tailored to ensure that the results are not biased by internal and external mass transfer limitations (Figs. S3–S7). An example of the mass and carbon balance closures using the H-ZSM-5/Al_2O_3 catalyst (Fig. S8) shows that *ca.* 28.7 wt% of the total mass was not identified, most likely due to the formation of heavy residues that remained in the reactor system [7].

The total carbon yields of aromatics (BTX and the other aromatics including ethylbenzene, naphthalene, and methyl naphthalenes) over the three fresh catalysts *versus* TOS are shown in Fig. 1. In general, the carbon yields of aromatics *versus* TOS show a maximum at about 3 h. At extended TOS, the aromatic carbon yields become negligible (*e.g.*, < 1 C.%) due to catalyst deactivation as a result of severe coking (*vide infra*). The initial increase is likely due to the time-dependent start-up of the fixed bed reactor [6,7]. The peak BTX carbon yield for the H-ZSM-5(28) catalyst is 34.7 C.%. Catalyst lifetime, defined as the time after start-up of the reactor to reach a BTX yield less than 1 C.% is 6.5 h. All in all, this leads to a total BTX productivity of 556 mg g^{-1} H-ZSM-5 (Table 1 and Fig. 1-left). The peak carbon yield of BTX and the total BTX productivity are considerably higher than found for the state-of-the-art values for H-ZSM-5(23) (*ca.* 28 C.% and 398 mg g^{-1} H-ZSM-5 [6]. A possible explanation is a difference in the SiO_2/Al_2O_3 molar ratio in the catalyst formulation, which is known to affect catalyst performance [12]. The values found here are the highest reported so far for GTA reactions performed at atmospheric pressure using pure glycerol as the feed and an unmodified H-ZSM-5 as the catalyst.

Compared to H-ZSM-5, Al_2O_3 is only marginally active for BTX formation and shows a peak BTX carbon yield of *ca.* 1.1 C.% (Table 1 and Fig. 1-right), which is close to values reported in the literature (0.7–4.3 C.% of BTX when using pure glycerol [19,22]). As such, the introduction of Al_2O_3 to H-ZSM-5 is expected to lower the BTX carbon yield due to a dilution effect. This is indeed observed for experiments using the H-ZSM-5/Al_2O_3 (60/40 wt%) catalyst, showing a peak BTX carbon yield of *ca.* 19.5 C.% (Table 1 and Fig. 1-middle). This value is lower than expected based on the intake and the peak yield of the individual catalyst components (21.1 C.%, turquoise line in

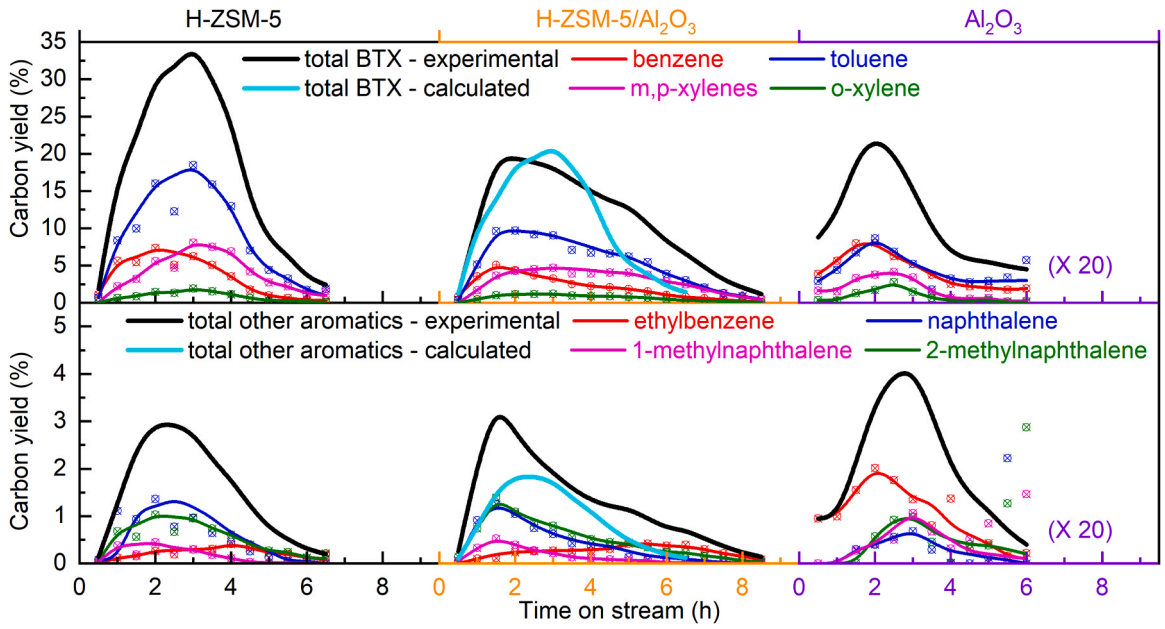

Fig. 1. Carbon yields of aromatics *versus* TOS over the fresh H-ZSM-5, Al_2O_3, and H-ZSM-5/Al_2O_3 catalysts. (The calculated curve for H-ZSM-5/Al_2O_3 catalyst is based on the intake and the performance of the individual components (H-ZSM-5 and Al_2O_3)).

Table 1
Performance of the catalysts for GTA.

	Peak carbon yield of BTX (C. %)	Catalyst life-time (h)	Total BTX productivity	
			(mg g^{-1} catalyst)	(mg g^{-1} H-ZSM-5)
H-ZSM-5 (fresh)	34.7	6.5	556	556
Al_2O_3 (fresh)	1.1	–	20	–
H-ZSM-5/Al_2O_3 (fresh)	19.5	8.5	426	710
H-ZSM-5/Al_2O_3 (fresh)	21.1[a]	–	342[a]	570[a]
H-ZSM-5/Al_2O_3 (regenerated-1)	20.5	11	580	967
H-ZSM-5/Al_2O_3 (regenerated-2)	22.5	9.5	569	945
H-ZSM-5/Al_2O_3 (regenerated-3)	20.0	9.5	439	732
H-ZSM-5/Al_2O_3 (regenerated-4)	19.0	7	311	518

[a] Calculated based on catalyst component intakes in the catalyst formulation and the catalyst performance of the individual components.

Fig. 1-middle). Such a decrease in the peak BTX carbon yield was also reported for an H-ZSM-5/Al_2O_3 catalyst containing a small amount of Al_2O_3 (10 wt%) [19].

Of interest is the peak carbon yield for the other aromatics such as ethylbenzene, naphthalene, and methyl naphthalenes when using the H-ZSM-5/Al_2O_3 catalyst (*ca.* 3.3 C.%), which is comparable to that over H-ZSM-5 (*ca.* 2.9 C.%, Fig. 1-left) and is higher than the calculated one (*ca.* 1.8 C.%, dotted curve in Fig. 1-middle).

Remarkably, a notable synergistic effect upon Al_2O_3 addition to the H-ZSM-5 catalyst was found for the catalyst lifetime and a significantly prolonged lifetime of the H-ZSM-5/Al_2O_3 catalyst to *ca.* 8.5 h was observed (Table 1 and Fig. 1-middle). This synergistic effect results in an enhanced total BTX productivity of *ca.* 710 mg g^{-1} H-ZSM-5 over the H-ZSM-5/Al_2O_3 catalyst (Table 1), which is by far higher than found for H-ZSM-5 alone and the calculated value (*ca.* 570 mg g^{-1} H-ZSM-5, Table 1) based on the weight average composition and the performance data for the individual catalyst components.

The selectivity to the individual BTX compounds is similar for H-ZSM-5 and H-ZSM-5/Al_2O_3 (Fig. S9), indicating a negligible effect of the Al_2O_3 binder addition on the selectivity of the reaction, rationalized by considering that the aromatization reaction mainly occurs in the pores of the H-ZSM-5 [19]. The main BTX component at peak BTX yield is toluene, followed by m-p-xylene. The selectivity of toluene and o-xylene is rather constant with TOS, while m,p-xylenes selectivity increases with TOS, at the expense of benzene (Fig. S9). This is most likely related to the gradual change in catalyst characteristics (microporosity and acidity) *versus* TOS, as recently postulated (reaction-zone migration model) [15].

3.2. *Reuse of the H-ZSM-5/Al_2O_3 catalyst for 5 reaction-regeneration cycles*

It has been shown above that the Al_2O_3 addition to H-ZSM-5 leads to a significantly prolonged catalyst lifetime and a higher total BTX productivity over the H-ZSM-5/Al_2O_3 catalyst for GTA. Therefore, it is of interest to further study the reusability of the H-ZSM-5/Al_2O_3 catalyst after regeneration. The used H-ZSM-5/Al_2O_3 catalyst was unloaded from the reactor after cooling to room temperature under an N_2 flow and then was regenerated by an *ex-situ* oxidative treatment in an oven under air at 680 °C for 12 h to remove the coke. The regenerated H-ZSM-5/Al_2O_3 catalyst was re-loaded to the reactor and was tested by following the same protocol used for the fresh catalyst. Five cycles of reaction-regeneration were performed and the catalyst performance of the fresh and regenerated catalysts is shown in Fig. 2.

In general, the peak BTX carbon yields (19.0–22.5 C.%, Table 1 (Fig. 2)) for the regenerated ones are about similar. Remarkably is the extended catalyst lifetimes for the catalyst after 1–3 regenerations (9.5–11 h, Table 1 and Fig. 2) compared to the fresh H-ZSM-5/Al_2O_3 catalyst. These extended lifetimes lead to an enhanced total BTX productivity of 732–967 mg g^{-1} H-ZSM-5 (Table 1) over the H-ZSM-5/Al_2O_3 (regenerated-1, −2, and −3) catalysts compared to that over the fresh H-ZSM-5/Al_2O_3 catalyst. After the 4th regeneration, though, catalyst lifetime is somewhat lower (*ca.* 7 h), resulting in a drop in the total BTX productivity (518 mg g^{-1} H-ZSM-5, Table 1). However, the catalyst performance over the H-ZSM-5/Al_2O_3 (regenerated-4) catalyst is still comparable to that for the fresh H-ZSM-5 (Table 1 and Fig. 2). Besides, a slightly higher m,p-xylene, and lower benzene selectivity are

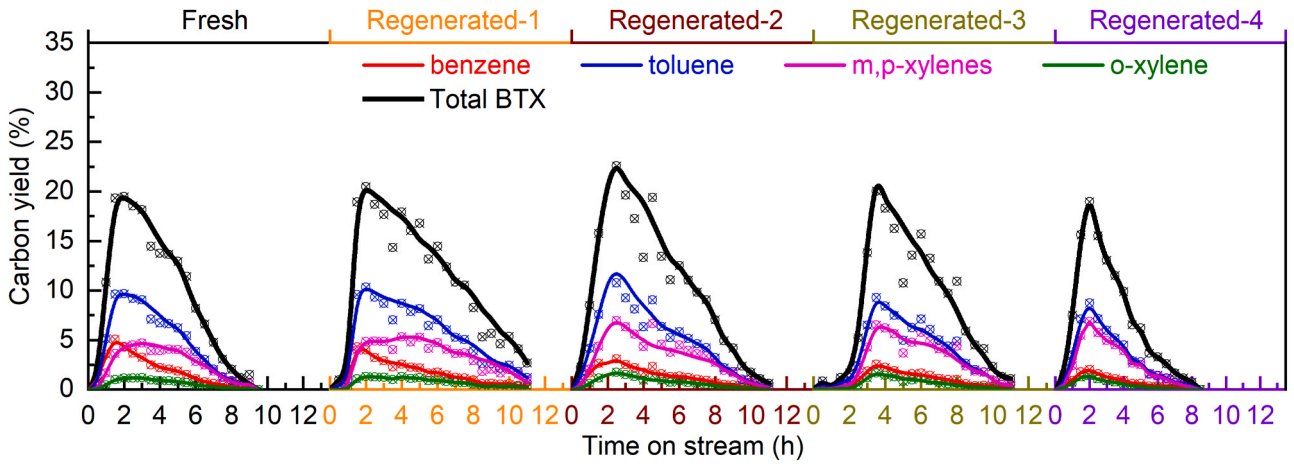

Fig. 2. Carbon yields of the total and individual BTX components *versus* TOS over the fresh and regenerated H-ZSM-5/Al_2O_3 catalysts.

obtained for the regenerated catalysts with an increase in regeneration cycles (Fig. S10), related to changes in the catalyst structure (*vide infra*). These results indicate good reusability of the H-ZSM-5/Al_2O_3 catalyst for GTA. It is actually much better than reported for H-ZSM-5 based catalysts in the literature, which typically show considerable irreversible deactivation after a few reaction-regeneration cycles [5,6,13,14,16,20].

In the following, catalyst performance (life-time, total BTX productivity, and regenerability, *vide supra*) for the H-ZSM-5/Al_2O_3 catalyst will be correlated to relevant catalyst characteristics (*e.g.* texture, acidity) upon the introduction of the Al_2O_3 binder and the results will be compared with H-ZSM-5 without a binder.

3.3. Characteristics of the fresh catalysts

To get the insights into the changes in catalyst characteristics by the introduction of the Al_2O_3 binder to H-ZSM-5, the three fresh H-ZSM-5,

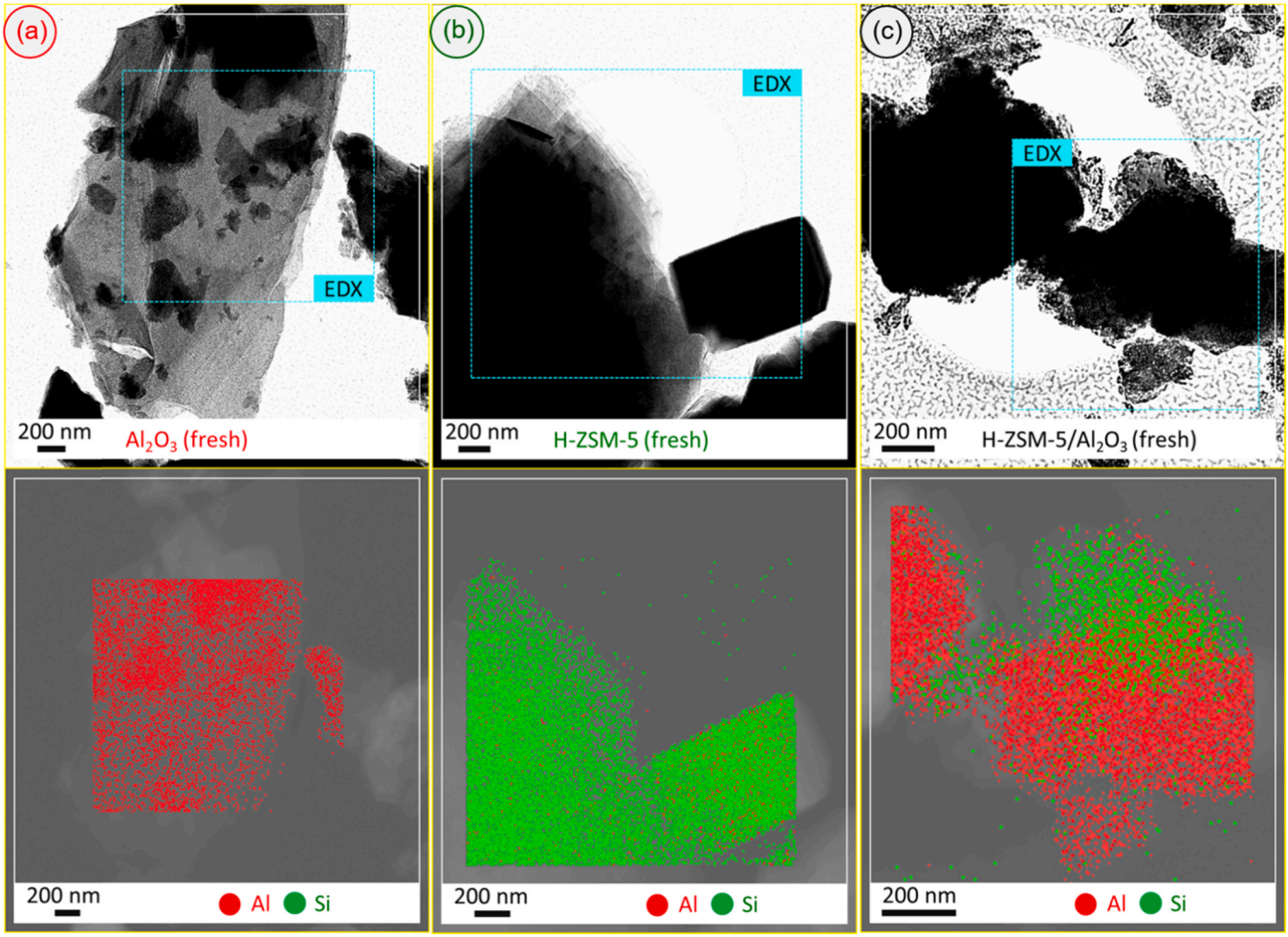

Fig. 3. TEM images and elemental (Al and Si) maps of the fresh (a) Al_2O_3, (b) H-ZSM-5, and (c) H-ZSM-5/Al_2O_3 catalysts.

Al_2O_3, and H-ZSM-5/Al_2O_3 catalysts were characterized in detail to determine the morphology (HR-TEM-EDX), textural property (N_2 and Ar physisorption), crystallinity (XRD), acidity (NH_3-TPD and pyridine-IR), and framework characteristics (^{27}Al and ^{29}Si MAS ssNMR).

3.3.1. *HR-TEM-EDX*

The EDX mapping of the H-ZSM-5/Al_2O_3 catalyst (Fig. 3-bottom-c and **S5**-left) shows two different zones with concentrated Al (red) and Si (green) elements, related to Al_2O_3 (Fig. 3-bottom-a) and H-ZSM-5 (Fig. 3-bottom-b) particles respectively. This is also reflected in the TEM image of the H-ZSM-5/Al_2O_3 catalyst (Fig. 3-top-c), showing the combination of Al_2O_3 (grey) and H-ZSM-5 (black) particles, which are in line with their individual TEM images (Fig. 3-top-a and b). Therefore, these results indicate the existence of an intimate, connected structure between the Al_2O_3 binder and H-ZSM-5 in the H-ZSM-5/Al_2O_3 catalyst [19]. Semi-quantified results (Table S1) show that the SiO_2 /Al_2O_3 molar ratio of H-ZSM-5 is *ca.* 28.4, in agreement with the XRF analysis (*ca.* 27.8, Table S1) and close to its specification (28) provided by the manufacturer. According to EDX and XRF analyses (Table S1), the H-ZSM-5/Al_2O_3 catalyst contains *ca.* 63 wt% H-ZSM-5 and 37 wt% Al_2O_3, which is in good agreement with the nominal intakes (60 and 40 wt%) used for the catalyst preparation.

3.3.2. *N_2 and Ar physisorption data*

The textural properties of the catalysts were analyzed by both Ar and N_2 physisorption [23]. Al_2O_3 shows the typical features of Type-IV N_2 adsorption-desorption isotherms (Fig. 4-left-a) [24] and a BJH mesopore size distribution of 3–20 nm (centered at *ca.* 5.5 nm, Fig. 4-right-a) was derived from the data, in agreement with those for γ-Al_2O_3 prepared by the calcination of boehmite [25]. The N_2 adsorption-desorption isotherms of H-ZSM-5 (Fig. 4-A-b) show a combination of Type I and Type IV [24] isotherms, related to N_2 adsorption in the micro-pores and inter-crystalline voids of H-ZSM-5 [26]. The latter shows a BJH mesopore size distribution of 3–5 nm (centered at *ca.* 3.8 nm, Fig. 4-right-d), in agreement with the literature [5,27]. The micro-pores show a NLDFT micropore size distribution of 0.4–0.6 nm (centered at *ca.* 0.51 nm, Fig. 4-middle-d), in agreement with the sizes of straight (*ca.* 0.54 × 0.56 nm) and sinusoidal (*ca.* 0.51 × 0.55 nm) channels in an MFI-type zeolite [6,28]. The other two peaks in the micro-pore size range of 0.7–1 nm and < 0.44 nm (Fig. 4-middle-d) are most likely the artifacts attributed to (i) an adsorbent phase transition (from fluid to crystalline) and (ii) pore coverage (from mono- to multilayer) [29]. As expected, the H-ZSM-5/Al_2O_3 catalyst shows the combination of the features of (i) the isotherms originated from the individual H-ZSM-5 ($P/P_0 < 0.1$) and Al_2O_3 ($P/P_0 > 0.4$) components (Fig. 4-left-g), (ii) an NLDFT micropore

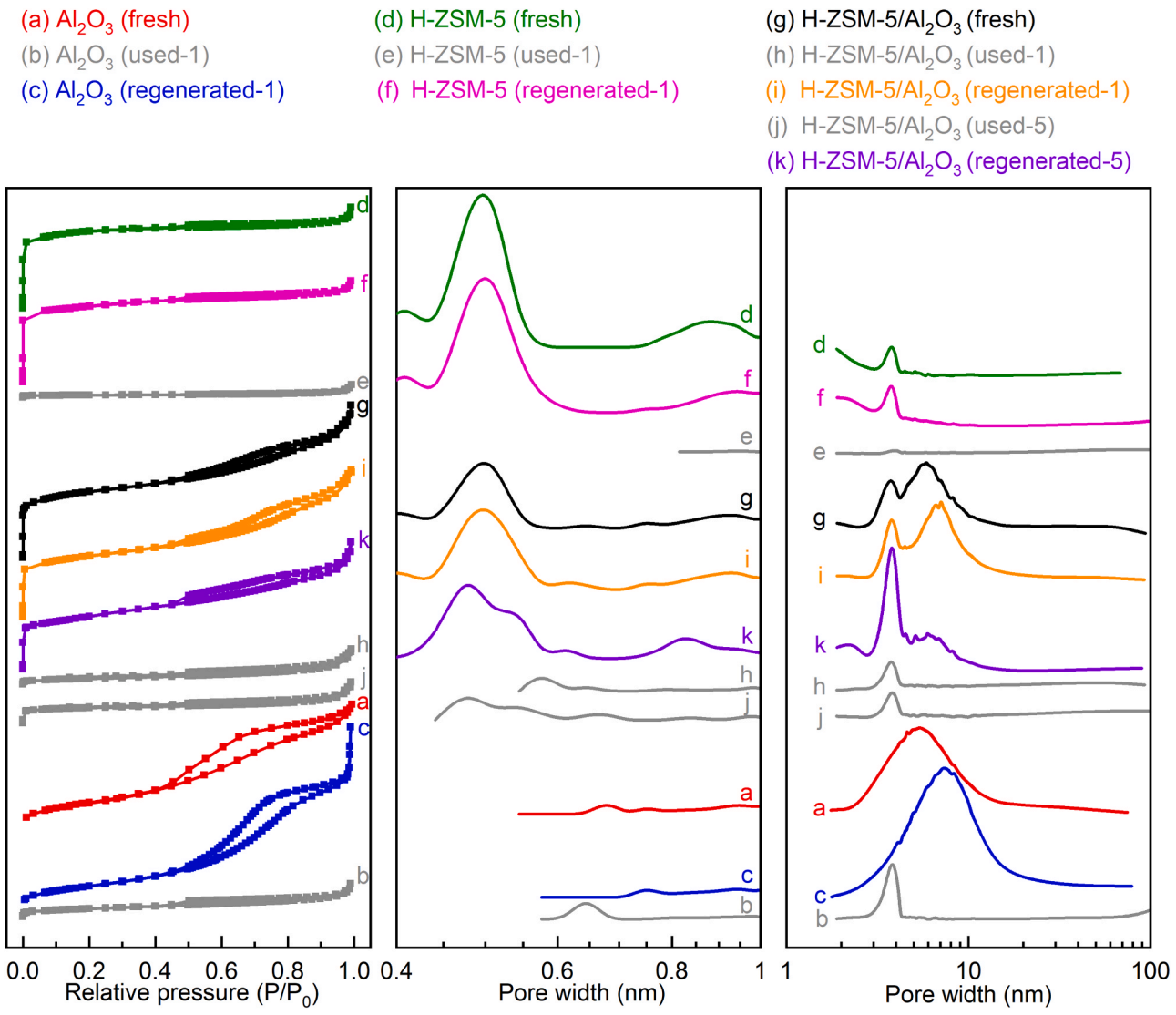

Fig. 4. N_2 adsorption-desorption isotherms (left), NLDFT micro-pore size distribution (middle), and BJH meso-pore size distribution (right) of the fresh, used, and regenerated Al_2O_3, H-ZSM-5, and H-ZSM-5/Al_2O_3 catalysts.

size distribution originating from H-ZSM-5 (Fig. 4-middle-g), and (iii) a bimodal BJH mesopore size distribution originating from H-ZSM-5 (centered at *ca.* 3.8 nm) and Al_2O_3 (centered at *ca.* 5.7 nm, Fig. 4-right-g).

Compared to H-ZSM-5, the H-ZSM-5/Al_2O_3 catalyst shows a lower specific surface area (S_{BET}, 288 *vs.* 353 $m^2\ g^{-1}$, Table 2), attributed to the dilution effect of the Al_2O_3 binder, which has a lower S_{BET} (171 $m^2\ g^{-1}$, Table 2) [30]. The experimental S_{BET} data is in line with that based on the calculated value according to the catalyst composition (288 *vs.* 286 $m^2\ g^{-1}$, Table 2). This indicates that the specific surface area of H-ZSM-5/Al_2O_3 is not significantly changed upon the addition of the Al_2O_3 binder. The total pore volume of H-ZSM-5/Al_2O_3 is higher than that of H-ZSM-5 (V_{pore}, 0.27 *vs.* 0.19 $cm^3\ g^{-1}$, Table 2), again, attributed to a dilution effect by introduction of the Al_2O_3 binder with a high V_{pore} (0.28 $cm^3\ g^{-1}$, Table 2). Moreover, the experimental V_{pore} of the H-ZSM-5/Al_2O_3 catalyst is higher than the calculated value according to the catalyst composition (0.27 *vs.* 0.23 $cm^3\ g^{-1}$, Table 2), most likely associated with newly-formed inter-particle pores during the catalyst preparation from the individual components.

The NLDFT model (Model # 251) is typically used to determine micropore volumes in zeolites for pores < 30 nm [21], For H-ZSM-5, the micropore volume (NLDFT $V_{micropore}$, 0.21 $cm^3\ g^{-1}$, Table 2) was close to literature data for H-ZSM-5(23) (*ca.* 0.20 $cm^3\ g^{-1}$) [6,15]. Considering the micro- and mesopore size distribution of H-ZSM-5 (Fig. 4-middle and right-d), this NLDFT $V_{micropore}$ represents the volume of the micropores (0.4–0.6 nm) of H-ZSM-5.

The addition of alumina to H-ZSM-5 leads to a slightly higher NLDFT $V_{micropore}$ value (0.27 $cm^3\ g^{-1}$, Table 2). This includes the volume of the micropores (0.4–0.6 nm) of H-ZSM-5 and also the mesopores (3–20 nm) of Al_2O_3. However, the NLDFT model is not suitable to determine the changes in the volume of the micropores (0.4–0.6 nm) of H-ZSM-5 upon the addition of the Al_2O_3 binder. As such, the NLDFT micropore size distribution curves of H-ZSM-5 and the H-ZSM-5/Al_2O_3 catalysts were plotted at the same baseline and are shown in Fig. S11. For the H-ZSM-5/Al_2O_3 catalyst, the experimental NLDFT micropore size distribution intensity (Fig. S11-c) is lower than the calculated one bases on composition (Fig. S11-d). These data indicate a reduction of the volume of the micropores (0.4–0.6 nm) of H-ZSM-5 in the H-ZSM-5/Al_2O_3 catalyst by the addition of the Al_2O_3 binder. This is most likely due to the a partly coverage of the micropores by the interaction of an H-ZSM-5 particle with Al_2O_3 particles.

3.3.3. XRD

The XRD pattern of H-ZSM-5 (Fig. S12-ii-a) is in line with those for H-ZSM-5 with a SiO_2/Al_2O_3 molar ratio of 23–280 [6,31] and shows the two featured diffraction peaks (♥) at $2\theta = ca.\ 7.9°$ and 8.9° for the [011] and [200] planes of an MFI-type zeolite [32]. The XRD pattern of Al_2O_3 (Fig. S12-i-a) shows the typical XRD features of γ-Al_2O_3 (ICDD: 00–029–0063) [33]. The intensity of the XRD pattern of Al_2O_3 is considerably lower than that of H-ZSM-5 (Fig. S13), in agreement with the literature [34]. This indicates that the Al_2O_3 binder has a by far lower crystallinity compared to the H-ZSM-5 zeolite. As such, the XRD pattern of the H-ZSM-5/Al_2O_3 catalyst (Fig. S12-iii-a) mainly shows the XRD features of H-ZSM-5. The height of the XRD peak (♣) at $2\theta = ca.$ 24.37° was used to calculate the relative crystallinity of the H-ZSM-5/Al_2O_3 catalyst (Eq. 4), which is *ca.* 100% (Table 2). These results indicate that the crystalline structure of H-ZSM-5 is hardly changed by the addition of the Al_2O_3 binder.

3.3.4. NH_3-TPD and pyridine-IR

The NH_3-TPD profile of H-ZSM-5 (Fig. S14-ii-a) shows a bimodal acidity distribution for the weak (centered at *ca.* 210 °C) and strong (centered at *ca.* 410 °C) acidic sites [5,35], in good agreement with those for H-ZSM-5 zeolites with a SiO_2/Al_2O_3 molar ratio of 23–280 [5,6,35,36]. The total acidity of H-ZSM-5 is *ca.* 1387 μmol $NH_3\ g^{-1}$ H-ZSM-5 (Table 2) when using the NH_3-TPD profile in a temperature

Table 2
Characterization of the catalysts.

Catalyst		S_{BET}[a] ($m^2\ g^{-1}$)	V_{pore}[a] ($cm^3\ g^{-1}$)	NLDFT $V_{micropore}$[b] ($cm^3\ g^{-1}$)	Relative crystallinity[c] (%)	Acidity[d] (μmol pyridine g^{-1} sample)				Acidity[e] (μmol NH_3 g^{-1} sample)	Carbon content[f] (wt%)	Coke content[g] (wt%)	T_M of DTG[g] (°C)
						Brønsted acid (B)	Lewis acid (L)	B+L	B/L				
H-ZSM-5	Fresh	353	0.19	0.21	100	714	143	857	5.0	1387	–	–	–
	Used-1	10	0.003	0.05	–	–	–	–	–	61	11.2	12.4	614
	Regenerated-1	330	0.19	0.27	90	–	–	–	–	591	–	–	–
Al_2O_3	Fresh	171	0.28	0.20	–	0	97	97	0.0	332	–	–	–
	Used-1	39	0.05	0.09	–	–	–	–	–	204	24.6	26.0	527
	Regenerated-1	143	0.28	0.24	–	–	–	–	–	299	–	–	–
H-ZSM-5/Al_2O_3	Fresh	288	0.27	0.27	100	469	215	684	2.2	1051	–	–	–
	Fresh	286[h]	0.23[h]	0.21[h]	100[h]	450[h]	126[h]	576[h]	3.6[h]	997[h]	–	–	–
	Used-1	27	0.05	0.05	–	–	–	–	–	177	19.2	20.5	554
	Regenerated-1	268	0.28	0.25	98	164	183	347	0.9	635	–	–	–
	Used-5	65	0.06	0.06	–	–	–	–	–	115	14.9	16.0	587
	Regenerated-5	232	0.22	0.22	60	45	84	130	0.5	304	–	–	–

[a]N_2 adsorption-desorption at 77 K, [b]Ar adsorption-desorption at 87 K, [c]XRD, [d]Pyridine-IR, [e]NH_3-TPD, [f]CHN elemental analysis, [g]TG-DTG (T_M is the temperature reaching a maximum weight loss rate.), and [h]calculated based on catalyst component and the catalyst characteristics of the individual components.

range of 100–550 °C. This is in the range of 1120−1464 μmol NH_3 g^{-1} H-ZSM-5 reported for H-ZSM-5 zeolites with a SiO_2/Al_2O_3 molar ratio of 23–30 [6,36]. The Al_2O_3 binder only shows the presence of weak acidic sites (Fig. S14-i-a) and has a total acidity of *ca.* 332 μmol NH_3 g^{-1} Al_2O_3 (Table 2), which is considerably lower than that of H-ZSM-5 (Table 2), in agreement with the literature [37]. Accordingly, the NH_3-TPD profile of the H-ZSM-5/Al_2O_3 catalyst (Fig. S14-iii-a) mainly shows the NH_3-TPD features of H-ZSM-5, of which the intensity is slightly higher compared to the calculated NH_3-TPD curve according to the catalyst composition and the individual acidity of the components (Fig. S14-iii-dotted line). This indicates a slightly enhanced total acidity (1051 *vs.* 997 μmol NH_3 g^{-1} catalyst, Table 2) on the H-ZSM-5/Al_2O_3 catalyst, most likely attributed to a synergistic effect between the binder and H-ZSM-5, generating new acidic sites (*vide infra*).

To gain insights into this synergistic effect on the Brønsted and Lewis acid sites of H-ZSM-5/Al_2O_3 catalyst, the catalyst acidity was further analyzed by pyridine-IR analysis. The two bands centered at *ca.* 1545 and 1455 cm^{-1} in the pyridine-IR spectrum of H-ZSM-5 (Fig. 5-a), corresponding to the protonated pyridine and the C-CN vibrations of metal-coordinated pyridine [38], indicate the presence of both Brønsted and Lewis acid sites on H-ZSM-5 [5,18,26]. Al_2O_3 only contains Lewis acid sites (Fig. 5-b), of which the strength is considerably lower than that of H-ZSM-5 (97 *vs.* 143 μmol pyridine g^{-1} sample, Table 2). For the H-ZSM-5/Al_2O_3 catalyst, the intensity of peaks in the pyridine-IR spectrum (Fig. 5-c) is lower than that of H-ZSM-5, attributed to dilution. In agreement with the NH_3-TPD results discussed above, the total acidity (the sum of Brønsted and Lewis acidity) of H-ZSM-5/Al_2O_3 is higher than the calculated value based on the catalyst composition and the individual acidity of the components (684 *vs.* 576 μmol pyridine g^{-1} catalyst, Table 2). In addition, the difference between the experimental value and the calculated one for Lewis acidity (215 *vs.* 126 μmol pyridine g^{-1} sample, Table 2) is more significant than that for Brønsted acidity (469 *vs.* 450 μmol pyridine g^{-1} sample, Table 2). These results imply a synergistic effect between the binder and H-ZSM-5 on catalyst acidity and reveal that this effect is mainly due to an increase in Lewis acidity. This enhanced Lewis acidity was also reported for other H-ZSM-5 catalysts with Al_2O_3 as the matrix [39]. The formation of additional Brønsted acidic sites could be due to the migration of aluminum in the H-ZSM-5 - Al_2O_3 matrix [30].

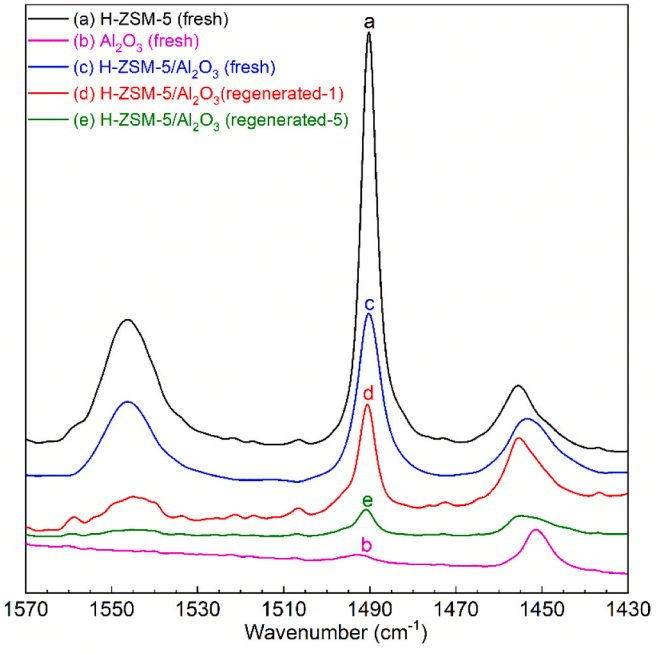

Fig. 5. Pyridine-IR spectra of the fresh and regenerated H-ZSM-5, Al_2O_3, and H-ZSM-5/Al_2O_3 catalysts.

3.3.5. ^{27}Al and ^{29}Si MAS ssNMR

Possible changes in the H-ZSM-5 framework upon the addition of the Al_2O_3 binder were analyzed by ^{27}Al and ^{29}Si MAS ssNMR. The ^{27}Al MAS ssNMR spectrum of Al_2O_3 (Fig. 6-left-a) shows two peaks at δ = *ca.* 12 and 68 ppm, corresponding to the octahedrally and tetrahedrally coordinated Al atoms in Al_2O_3, in agreement with literature data for γ-Al_2O_3 [40]. The ^{27}Al MAS ssNMR spectrum of H-ZSM-5 (Fig. 6-left-c) shows two peaks at δ = *ca.* 0 and 53 ppm, in line with H-ZSM-5 zeolites with a SiO_2/Al_2O_3 molar ratio between 23 and 150 [6,41]. These peaks are assigned to octahedrally coordinated extra-framework Al (abbreviated as EFAl) and tetrahedrally coordinated framework Al (abbreviated as FAl) [42] species, respectively. The NMR peak for the EFAl of H-ZSM-5 in the H-ZSM-5/Al_2O_3 catalyst is hardly visible due to strong overlap with the intense peak of octahedrally-coordinated Al of Al_2O_3 (Fig. 6-left-e). Besides, the peak for the FAl of H-ZSM-5 also partially overlaps with the tetrahedrally-coordinated Al of Al_2O_3 (Fig. 6-left-e). This hampers the use of ^{27}Al MAS ssNMR analysis to study changes in the H-ZSM-5 framework upon preparing the shaped H-ZSM-5/Al_2O_3 catalyst [43].

In this respect, ^{29}Si MAS ssNMR is more informative. The ^{29}Si MAS ssNMR spectrum of H-ZSM-5 (Fig. 6-right-c) and the H-ZSM-5/Al_2O_3 catalyst (Fig. 6-right-e) shows an intense peak (δ = *ca.* −113 ppm) with a weak shoulder (δ = *ca.* −106 ppm), which are generally assigned to the Si(4Si, 0Al) and Si(3Si, 1Al) species in the H-ZSM-5 framework [5,44]. Therefore, a reduction of the peak intensity of the resonance associated with Si(3Si, 1Al) is used as an indicator for dealumination of the H-ZSM-5 framework [6,45]. Accordingly, the ^{29}Si MAS ssNMR spectra of H-ZSM-5 and the H-ZSM-5/Al_2O_3 catalysts were plotted at the same baseline and with the similar height of the Si(4Si, 0Al) resonance and the result is shown in Fig. S15. The intensity of the Si(3Si, 1Al) resonance for H-ZSM-5/Al_2O_3 (Fig. S15-c) is slightly higher than that for H-ZSM-5 (Fig. S15-a), indicating Al migration from Al_2O_3 to the H-ZSM-5 framework in H-ZSM-5/Al_2O_3. This Al transfer to the H-ZSM-5 framework [46] leads to a decreased SiO_2/Al_2O_3 molar ratio of the H-ZSM-5 framework, resulting in a slightly enhanced Brønsted acidity [12,30], which is in good agreement with the pyridine-IR results (Table 2).

3.4. Characteristics of the used catalysts after reaction

To get insights into the changes in catalyst properties after use for BTX formation (550 °C for a TOS of 6.5–8.5 h, Fig. 1 and Table 1), the used H-ZSM-5, Al_2O_3, and H-ZSM-5/Al_2O_3 catalysts were characterized using the same characterization protocols as used for the fresh catalysts (*vide supra*). Besides, TG-DTG (Fig. S16) and elemental analyses (Table 2) were performed for quantification of the amount of coke deposited on the used catalysts.

The TG curve of the H-ZSM-5 (used-1) catalyst (Fig. S16-top-b) shows a significant weight loss at a temperature of 450–650 °C, corresponding to the coke removal *via* oxidation. The coke content on the H-ZSM-5 (used-1) is *ca.* 12.4 wt% (Table 2), in agreement with the elemental analysis result showing a carbon content of 11.2 wt% (Table 2). The DTG curve of the H-ZSM-5 (used-1, Fig. S16-bottom-b) shows a maximum weight loss rate (T_M) at *ca.* 614 °C (Table 2). These values for the coke content and T_M for the H-ZSM-5 (used-1) catalyst in this study are in the range of the reported values (8–15 wt% and 550–650 °C) for the conversion of glycerol to BTX using unmodified H-ZSM-5 [6,10,15–17,19].

The coke content on the Al_2O_3 (used-1) catalyst is much higher than found for H-ZSM-5 (used-1) and is about 26.0 wt% (or 24.6 wt% of carbon, Fig. S16-top-a and Table 2). This indicates that the Al_2O_3 binder has a much higher coke accommodation capacity than H-ZSM-5, most likely due to the mesoporous nature of Al_2O_3 (Fig. 4 and Table 2). Comparatively, the T_M for the Al_2O_3 (used-1) is by far lower than for H-

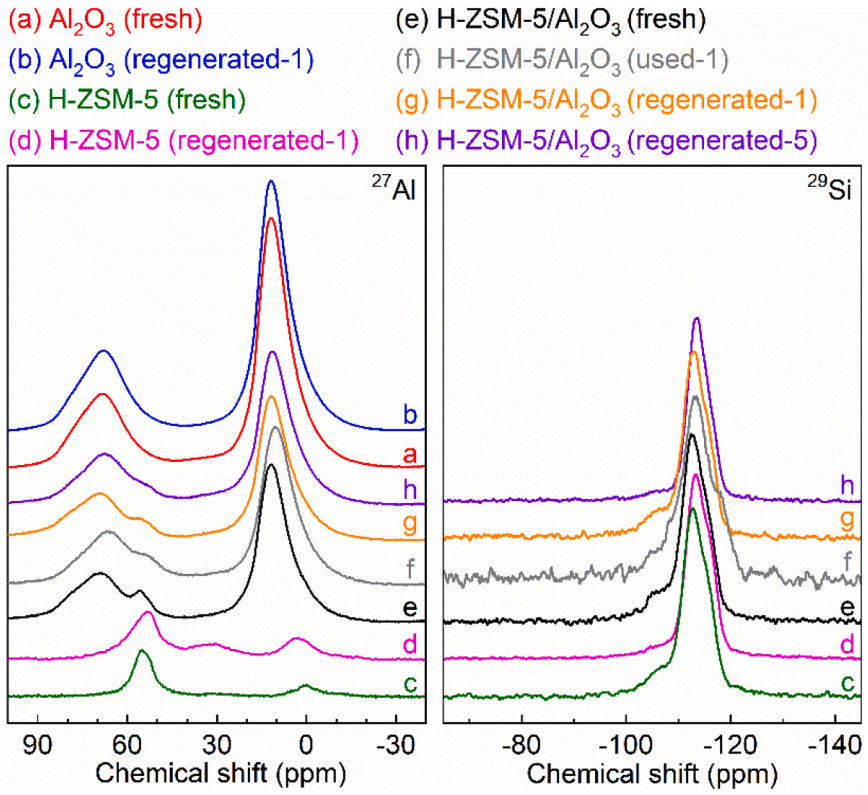

Fig. 6. ^{27}Al and ^{29}Si MAS ssNMR spectra of the fresh, used, and regenerated H-ZSM-5, Al_2O_3, and H-ZSM-5/Al_2O_3 catalysts.

ZSM-5 (used-1, 527 *vs.* 614 °C, Table 2), indicating that the coke formed on Al_2O_3 is softer than on H-ZSM-5. This is in good agreement with the XRD results, showing that graphitic coke [5,6,15] is formed on the H-ZSM-5 (used-1, indicated by the XRD peaks ∇, Fig. S12-ii-b) while the coke formed on Al_2O_3 (used-1) is amorphous in nature (Fig. S12-i-b).

The H-ZSM-5/Al_2O_3 (used-1) catalyst shows an intermediate coke content (*ca.* 20.5 wt% of coke or 19.2 wt% of carbon, Fig. S16-top-c and Table 2). EDX mapping of H-ZSM-5/Al_2O_3 (used-1) (Fig. 7-a) reveals that catalyst particles enriched with Al_2O_3 (Spectra 2–3, Fig. 7-a) have a higher carbon content than those with fewer Al_2O_3 particles (Spectrum 1, Fig. 7-a). This indicates that the coke is predominantly located on the Al_2O_3 binder, in agreement with the literature [39]. The T_M of DTG is 554 °C (Fig. S16-bottom-c and Table 2) and the coke is highly crystalline (Fig. S12-iii-b), similar to the coke formed when using the H-ZSM-5 catalyst (Fig. S12-ii-b). These results suggest that the coke is most likely formed in the pores of H-ZSM-5 and then migrates to the Al_2O_3 with TOS [47].

Coke deposition also has a significant effect on the catalyst porosity and acidity (Table 2), which are essential for aromatization [48] and shape-selectivity [49]. The H-ZSM-5 (used-1) catalyst shows a strong reduction in S_{BET}, V_{pore}, NLDFT micropore size distribution, and total acidity compared to the fresh one (Fig. 4-e and Table 2). These changes due to coke formation are also the cause for the experimentally observed catalyst deactivation pattern, giving rise to negligible BTX formation after a TOS of 6.5 h (Fig. 1-left). Similar trends are also observed for the H-ZSM-5/Al_2O_3 (used-1) catalyst, losing *ca.* 90% of S_{BET}, *ca.* 81% of V_{pore}, and *ca.* 83% of total acidity compared to the fresh one (Table 2).

3.5. Characteristics of the regenerated catalysts after one cycle of reaction-regeneration

Severe coke deposition during reaction covers the catalyst surface and blocks the micro-and mesopores [7], leading to a significant decrease in micro-porosity and acidity of the used catalysts (*vide supra*). The used catalysts were regenerated by an *ex-situ* oxidative treatment in air at 680 °C for 12 h. These catalyst regeneration conditions were based on the TG-DTG results. Coke removal after regeneration is confirmed by the EDX and XRD analyses, showing negligible carbon content in the regenerated H-ZSM-5/Al_2O_3 catalysts (Fig. S17-middle and right) and the disappearance of the coke related XRD peaks (∇ and ◊, Fig. S12-ii-c, -iii-c and -e). The regenerated H-ZSM-5, Al_2O_3, and H-ZSM-5/Al_2O_3 catalysts were characterized in detail using the same protocol as used for the characterization of the fresh catalysts (*vide supra*).

After one reaction-regeneration cycle, the textural properties (S_{BET}, V_{pore}, and NLDFT micro-and BJH meso-pore size distributions, Table 2 and Fig. 4-i) and the crystalline structure (Fig. S12-iii-c) of the H-ZSM-5/Al_2O_3 (regenerated-1) catalyst are mostly recovered. Besides, a negligible crystallinity decrease (*ca.* 2%, Table 2) is detected. It is of interest to compare these findings with that for H-ZSM-5 without a binder. The decrease in total acidity for H-ZSM-5/Al_2O_3 (regenerated-1, 40%) is considerably lower than that for H-ZSM-5 (regenerated-1, 57%, Table 2). These results indicate that the addition of the Al_2O_3 binder to the H-ZSM-5/Al_2O_3 catalyst has a positive effect on catalyst properties after reaction/regeneration.

NH_3-TPD profiles of H-ZSM-5 (regenerated-1) and H-ZSM-5/Al_2O_3 (regenerated-1) show that the peak for the strong mainly Brønsted acidic sites (centered at *ca.* 410 °C) [35], is remarkably decreased compared to the weak acidic sites (Fig. S14-ii-c and iii-c). This is in good accordance with the pyridine-IR of the H-ZSM-5/Al_2O_3 (regenerated-1) catalyst, showing that the decrease in the Brønsted acidity is by far higher than that in the Lewis acidity (65 *vs.* 15%, Table 2). This leads to a decreased Brønsted acidity/Lewis acidity (B/L) molar ratio for H-ZSM-5/Al_2O_3 (regenerated-1) catalyst compared to H-ZSM-5/Al_2O_3 (fresh) catalyst (B/L of 0.9 *vs.* 2.2, Table 2). These results imply that the number of Brønsted acidic sites in H-ZSM-5/Al_2O_3 is lowered at a faster rate than the Lewis acidic sites during the reaction-regeneration cycle. This is in agreement with regeneration studies for H-ZSM-5(23) [6] and H-ZSM-5(23)/bentonite [5] for GTA. Notably, the H-ZSM-5/Al_2O_3 catalyst in this study shows a lower

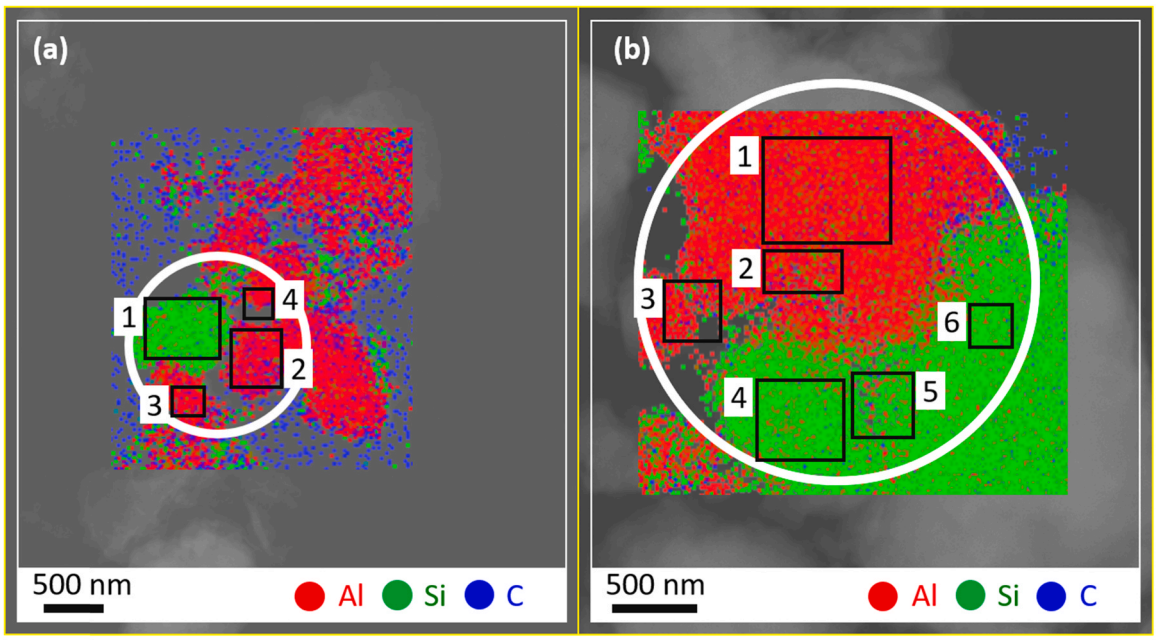

	C (mol.%)	Al (mol.%)	Si (mol.%)	SiO_2/Al_2O_3 (mol. : mol.)
(a) H-ZSM-5/Al_2O_3 (Used-1)				
Spectrum 1	25.3	7.2	67.6	18.87
Spectrum 2	54.6	43.4	2.1	0.10
Spectrum 3	49.3	48.5	2.2	0.09
Spectrum 4	36.8	59.1	4.0	0.14
(b) H-ZSM-5/Al_2O_3 (Used-5)				
Spectrum 1	21.77	69.32	8.92	0.26
Spectrum 2	24.99	64.57	10.44	0.32
Spectrum 3	22.97	68.63	8.4	0.24
Spectrum 4	10.11	10.82	79.07	14.62
Spectrum 5	9.2	11.24	79.56	14.16
Spectrum 6	8.58	8.98	82.44	18.36

Fig. 7. Elemental (Al and Si) maps of the used H-ZSM-5/Al_2O_3 catalysts. (The white circle represent holes in the carbon-coated copper grid).

reduction in Brønsted acidity compared to the unmodified H-ZSM-5(23) [6] (65 *vs.* 78%), indicating that the Al_2O_3 binder reduces the rate of irreversible deactivation of Brønsted acidic sites.

The ^{29}Si MAS ssNMR spectrum of the H-ZSM-5/Al_2O_3 (regenerated-1) catalyst (Fig. 6-g) is very similar to that of the fresh one (Fig. 6-e), though there is a very slight decrease in the intensity of the peak Si(3Si, 1Al) (Fig. S15-d *vs.* -c). This indicates that some minor dealumination occurred after one reaction-regeneration cycle. However, the H-ZSM-5 (regenerated-1) catalyst without the binder shows a by far higher level of dealumination (Fig. S15-b *vs.* -a). These results indicate that the addition of the Al_2O_3 binder to the H-ZSM-5 inhibits the extent of dealumination of the H-ZSM-5 framework during a reaction-regeneration cycle. Therefore, the decreased acidity, particularly the Brønsted acidity, of the H-ZSM-5/Al_2O_3 (regenerated-1) catalyst is most likely predominantly due to a thermal effect [50] during the first cycle reaction-regeneration.

3.6. Characterization of used catalysts after five reaction/regeneration cycles

The H-ZSM-5/Al_2O_3 (used-5) shows a lower coke content (*ca.* 16.0 wt% of coke or 14.9 wt% of carbon, Fig. S16-top-d and Table 2) compared to H-ZSM-5/Al_2O_3 (used-1), likely due to the decreased catalyst acidity after 5 recycles (Table 2). However, the coke on H-ZSM-5/Al_2O_3 (used-5) is harder compared to that on H-ZSM-5/Al_2O_3 (used-1), as indicated by the presence of graphitic coke with a high crystallinity (Fig. S12-iii-d) and the higher T_M (*ca.* 587 °C, Fig. S16-bottom-a and Table 2). EDX mapping of H-ZSM-5/Al_2O_3 (used-5, Fig. 7-b) also shows that a non-homogeneous distribution of carbon, which has a higher concentration in the particles enriched in Al_2O_3 (Spectra 1–3, Fig. 7-b *versus* Spectra 4–6, Fig. 7-b), in line with the findings for H-ZSM-5/Al_2O_3 (used-1) (Fig. 7-a). Besides, H-ZSM-5/Al_2O_3 (used-5) catalyst loses *ca.* 89% of total acidity of the fresh one (Table 2), higher than H-

ZSM-5/Al_2O_3 (used-1) catalyst. Therefore, these results indicate a further deterioration in catalyst characteristics with the number of reaction/regeneration cycles.

3.7. Characterization of regenerated catalysts after five cycles of reaction-regeneration

EDX mapping of H-ZSM-5/Al_2O_3 (regenerated-5) shows the presence of closely connected H-ZSM-5 and Al_2O_3 particles (Figs. S17-right). However, different from the H-ZSM-5/Al_2O_3 (regenerated-1) catalyst, the H-ZSM-5/Al_2O_3 (regenerated-5) catalyst shows a *ca.* 20% decrease in textural properties (S_{BET} and V_{pore}, Table 2) and a *ca.* 40% decrease in crystallinity (Table 2) compared to fresh H-ZSM-5/Al_2O_3. The BJH mesopore size distribution of H-ZSM-5/Al_2O_3 (regenerated-5, Fig. 4-right-k) shows a dramatic increase in the intensity of the peak centered at *ca.* 3.8 nm and simultaneously a decrease in the intensity of the peak centered at *ca.* 5.8 nm. The latter corresponds to the mesopores in the Al_2O_3 binder (*vide supra*). Besides, the NLDFT micro-pore size distribution of the H-ZSM-5/Al_2O_3 (regenerated-5) catalyst (Fig. 4-middle-k) shows a new shoulder at *ca.* 0.55 nm beside the peak centered at *ca.* 0.51 nm.

These results indicate that after 5 reaction-regeneration cycles, the mesoporous structure of the Al_2O_3 binder partly collapses partly, affecting the microporous structure of H-ZSM-5. In addition, H-ZSM-5/Al_2O_3 (regenerated-5) shows a significant reduction in total acidity of *ca.* 71% by NH_3-TPD and 81% by pyridine-IR (Table 2). Furthermore, the B/L ratio of H-ZSM-5/Al_2O_3 (regenerated-5) is only 0.5 (Table 2), which is by far lower than those for H-ZSM-5/Al_2O_3 (fresh, 2.2) and (regenerated-1, 0.9). Besides the thermal effect [50] during the five cycles of reaction-regeneration, the further reduction in acidity of H-ZSM-5/Al_2O_3 (regenerated-5) may also be due to the dealumination of the H-ZSM-5 framework. This is confirmed by a ^{29}Si MAS ssNMR spectrum of the H-ZSM-5/Al_2O_3 (regenerated-5) catalyst (Fig. 6-h), showing a clear decrease in the intensity of the peak Si(3Si, 1Al) compared to H-ZSM-5/Al_2O_3 (fresh, Fig. S15-e *vs.* -c). These results imply that the catalyst characteristics of the H-ZSM-5/Al_2O_3 catalyst such as textural properties, crystallinity, acidity (Brønsted acidity in particular), and the framework, deteriorate with the number of reaction-regeneration cycles. Nevertheless, compared to unmodified H-ZSM-5 [6] and H-ZSM-5/bentonite [5], the addition of the Al_2O_3 binder to the H-ZSM-5/Al_2O_3 catalyst has a remarkable positive effect on properties and reduces the rate of irreversible deactivation.

3.8. Discussion

Both reversible and irreversible deactivation has been observed when using H-ZSM-5-based catalysts for GTA. Reversible deactivation is due to coke formation during the reaction and, as a result, blockage of active sites. A previous study on coke characteristics by various analysis techniques has shown that coke formation involves the initial formation of oxygenated coke followed by dehydration and hydrogen transfer to form a more aromatic coke [51]. Nevertheless, coke may be removed very effectively using an oxidative regeneration procedure [10,16]. Irreversible deactivation is typically observed after (multiple) reaction-regeneration cycle(s) and is related to the loss of acidity, dealumination of the H-ZSM-5 framework, and partial collapse of the crystalline structure.

We here show that the addition of the Al_2O_3 binder in the H-ZSM-5/Al_2O_3 catalyst has a positive effect on catalyst stability as is evident from a prolonged life-time to 8.5 h (*vs.* 6.5 h for the H-ZSM-5 catalyst, Fig. 1), leading to an enhanced total BTX productivity of 710 mg g^{-1} H-ZSM-5 (*vs.* 556 mg g^{-1} H-ZSM-5 for the H-ZSM-5 catalyst, Scheme 1). A

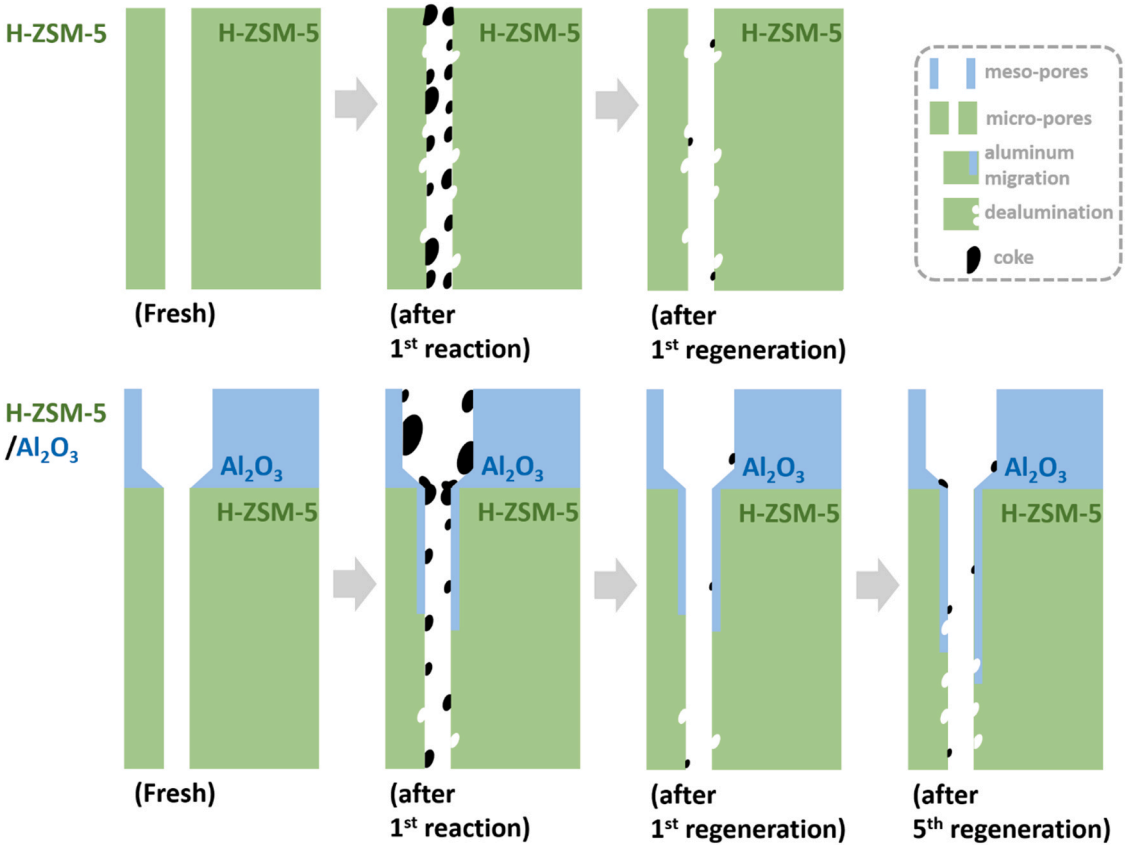

Scheme 1. Schematic representation of reversible and irreversible catalyst deactivation for the conversion of glycerol to BTX (top: H-ZSM-5 alone, bottom: H-ZSM-5/alumina).

possible explanation for this observation is transfer of the coke formed in the vicinity of the active acidic sites located in the micropores of H-ZSM-5 to the mesopores in Al_2O_3 and the newly formed mesopores (centered at *ca*. 5.7 nm, Fig. 4-right-g) after the addition of the Al_2O_3 binder (Scheme 1). Coke migration has been postulated in the literature for zeolite-binder combinations [39,47,52]. This hypothesis is supported by TEM-EDX measurements showing a non-homogeneous distribution of carbon deposits, with higher carbon content in the particles enriched with Al_2O_3 (Fig. 7).

In general, the turnover numbers (TONs) for H-ZSM-5-based catalysts for GTA are rather low *viz.* 8 $mol_{total\ BTX}\ mol_{acid\ site}^{-1}$ for crude glycerol conversion over an H-ZSM-5/bentonite (60/40 wt%) catalyst for a TOS of 4.7 h [5] and 13.6 $mol_{total\ BTX}\ mol_{acid\ site}^{-1}$ for pure glycerol conversion over a H-ZSM-5(23) zeolite catalyst for a TOS of 5 h [6]. The TON for the H-ZSM-5/Al_2O_3 catalyst reported here is 17.2 $mol_{total\ BTX}\ mol_{acid\ site}^{-1}$, which is a considerable improvement compared to the state of the art. In addition, this value is approximately 2.4 times higher than the value found for H-ZSM-5 without a binder. Thus, the addition of the Al_2O_3 binder has a positive effect on the TON for GTA.

Remarkably, after catalyst regeneration by an oxidative treatment of the used catalyst, the regenerated-1 catalyst shows a by far higher TON compared to the fresh H-ZSM-5/Al_2O_3 (60/40 wt%) catalyst (69.1 *vs.* 17.2 $mol_{total\ BTX}\ mol_{acid\ site}^{-1}$). This improved TON for GTA over the H-ZSM-5-based catalyst after regeneration was also observed for the H-ZSM-5/bentonite (60/40 wt%) catalyst (TONs of 8 for fresh and 41 $mol_{total\ BTX}\ mol_{acid\ site}^{-1}$ after regeneration for 11 times [5]. A possible explanation is that only a threshold number of acidic sites is required for BTX formation and that additional acidic sites only lead to excessive coke formation. [5,15].

The addition of the Al_2O_3 binder to the H-ZSM-5/Al_2O_3 catalyst also has a positive effect on the extent of irreversible catalyst deactivation upon multiple reaction-regeneration cycles. The regenerated H-ZSM-5/Al_2O_3 catalyst after 3 times of regeneration shows an even slightly better catalyst performance compared to the fresh one (*e.g.*, peak BTX carbon yield of 20.0 *vs*. 19.5%, life-time of 9.5 *vs*. 8.5 h, and total BTX productivity of 732 *vs*. 710 mg g^{-1} H-ZSM-5, Table 1 and Fig. 2). This is an unprecedented observation as typically considerably irreversible deactivation during 2–4 reaction-regeneration cycles is observed for the conversion of glycerol to BTX using zeolitic catalysts (Table S2) [5,6,13,14,16,20]. This enhanced reusability of the H-ZSM-5/Al_2O_3 catalyst is due to the addition of Al_2O_3 binder, which significantly slows down the rate of irreversible deactivation most likely *via* the aluminum migration from the binder to H-ZSM-5 framework (Scheme 1) to compensate for dealumination of the H-ZSM-5 framework.

Nevertheless, some irreversible deactivation was also observed for the H-ZSM-5/Al_2O_3 (regenerated-4) catalyst, leading to a reduced catalyst lifetime of 7 h (*vs*. 8.5 h for the fresh H-ZSM-5/Al_2O_3 catalyst Table 1 and Fig. 2). This is most likely related to the relatively low (hydrothermal) stability of the mesopores of Al_2O_3 and dealumination of the H-ZSM-5 framework after the long-time exposure with steam (under catalysis and regeneration conditions), which result in a reduction in micropore volume and a reduction in acidic sites.

4. Conclusions

A granular H-ZSM-5/Al_2O_3 (60/40 wt%) catalyst was synthesized, characterized, and used for the catalytic conversion of glycerol to aromatics. The addition of Al_2O_3 was shown to have a positive effect on catalyst performance compared to the unmodified H-ZSM-5 catalyst such as (i) a high total BTX productivity of 710 mg g^{-1} H-ZSM-5, which is the highest value for the conversion of pure glycerol to BTX reported so far; (ii) improved catalyst reusability as the catalyst shows very limited irreversible deactivation after 4 reaction-regeneration cycles, and (iii) a higher industrial relevance as shaping and binding is typically done in industry for zeolitic catalysts to improve catalyst characteristics and performance.

Detailed characterization studies were performed to get a better understanding of the positive effect of alumina on catalyst performance. The H-ZSM-5/Al_2O_3 catalyst shows the combined textural properties (N_2 isotherms, micro- and meso-pore size distribution) of the individual H-ZSM-5 and Al_2O_3 components The addition of the Al_2O_3 binder does not affect the catalyst surface area and the crystallinity of the H-ZSM-5 when compensating for dilution. However, other relevant characteristics are affected by the addition of the binder. For instance, (i) the total pore volume is increased due to newly-formed inter-particle pores, (ii) the micropore volume is decreased due to the coverage of the micropores and surface of H-ZSM-5 by Al_2O_3, and (iii) the total acidity (particularly the Lewis acidity) is increased due to the Al migration from Al_2O_3 to the H-ZSM-5 framework.

These findings provide clues to explain the improved performance of the H-ZSM-5/alumina combination compared to H-ZSM-5 alone. Prolonged catalyst lifetime is likely due to transfer of coke from the active sites in the zeolite to (i) the mesopores of the Al_2O_3 binder and (ii) the newly formed mesopores upon catalyst synthesis, providing additional space for coke. In addition, the extent of irreversible deactivation, among others caused by dealumination during reaction and regeneration, is most likely reduced due to the transfer of Al cations from Al_2O_3 to the zeolitic framework. However, irreversible deactivation cannot be eliminated fully and after multiple reaction-regeneration cycles some deactivation is observed, most likely due to partial collapse of the Al_2O_3 binder (reduction in mesoporosity) and the H-ZSM-5 framework (dealumination). This is likely due to the action of water/steam, which is formed in large amounts during the reaction as well as in the regeneration step. The prevention of irreversible deactivation will require special attention in the development of the active and regenerable industrial catalysts for GTA.

CRediT authorship contribution statement

Thomas Sjouke Kramer, Frederike Gerda Hiltje Klein, Anshu Chandel, Zhuorigebatu Tegudeer, Chuncheng Liu: Investigation, Writing – original draft. **Songbo He, Evgeny Pidko**: Supervision, Validation, Writing – review & editing. **Andre Heeres**: Conceptualization, Supervision, Validation, Writing – review & editing. **H.J. Heeres**: Conceptualization, Funding acquisition, Supervision, Validation, Writing – review & editing.

Declaration of Competing Interest

The authors declare that they have no known competing financial interests or personal relationships that could have appeared to influence the work reported in this paper.

Acknowledgments

We thank Nederlandse Organisatie voor Wetenschappelijk Onderzoek (NWO) for financial support (NWO-LIFT program, Grant No. 731.016.401). We also thank BIOBTX for the collaboration and valuable discussions. Dr. K.S.S. Gupta from the Leiden Institute of Chemistry at Leiden University, Dr. M.C.A. Stuart from the Electron Microscopy Facility at the University of Groningen, and J. van Dijken from the Zernike Institute for Advanced Materials at the University of Groningen are acknowledged for performing the MAS ssNMR, HR-TEM-EDX, and TG-DTG analyses.

Appendix A. Supporting information

Supplementary data associated with this article can be found in the online version at doi:10.1016/j.apcata.2021.118393.

References

[1] X. Luo, X. Ge, S. Cui, Y. Li, Bioresour. Technol. 215 (2016) 144–154, https://doi.org/10.1016/j.biortech.2016.03.042.
[2] C.H.C. Zhou, J.N. Beltramini, Y.X. Fan, G.Q.M. Lu, Chem. Soc. Rev. 37 (2008) 527–549, https://doi.org/10.1039/b707343g.
[3] P.S. Kong, M.K. Aroua, W. Daud, Renew. Sust. Energ. Rev. 63 (2016) 533–555, https://doi.org/10.1016/j.rser.2016.05.054.
[4] C.M. Lok, J. Van Doorn, G.A. Almansa, Renew. Sust. Energ. Rev. 113 (2019) 1–11, https://doi.org/10.1016/j.rser.2019.109248.
[5] S. He, I. Muizebelt, A. Heeres, N.J. Schenk, R. Blees, H.J. Heeres, Appl. Catal., B 235 (2018) 45–55, https://doi.org/10.1016/j.apcatb.2018.04.047.
[6] S. He, K. Zuur, D.S. Santosa, A. Heeres, C. Liu, E. Pidko, H.J. Heeres, Appl. Catal., B 281 (2021) 1–14, https://doi.org/10.1016/j.apcatb.2020.119467.
[7] S. He, F.G.H. Klein, T.S. Kramer, A. Chandel, Z. Tegudeer, A. Heeres, H.J. Heeres, ACS Sustain. Chem. Eng. 9 (2021) 1128–1141, https://doi.org/10.1021/acssuschemeng.0c06181.
[8] O. Muraza, Front. Chem. 7 (2019) 1–11, https://doi.org/10.3389/fchem.2019.00233.
[9] G. Li, E.A. Pidko, Chemcatchem 11 (2019) 134–156, https://doi.org/10.1002/cctc.201801493.
[10] T.Q. Hoang, X.L. Zhu, T. Danuthai, L.L. Lobban, D.E. Resasco, R.G. Mallinson, Energy Fuels 24 (2010) 3804–3809, https://doi.org/10.1021/ef100160y.
[11] Y. Xiao, A. Varma, ACS Energy Lett. 1 (2016) 963–968, https://doi.org/10.1021/acsenergylett.6b00421.
[12] S. Tamiyakul, W. Ubolcharoen, D.N. Tungasmita, S. Jongpatiwut, Catal. Today 256 (2015) 325–335, https://doi.org/10.1016/j.cattod.2014.12.030.
[13] F. Wang, W.Y. Xiao, L.J. Gao, G.M. Xiao, RSC Adv. 6 (2016) 42984–42993, https://doi.org/10.1039/c6ra03358j.
[14] W.Y. Xiao, F. Wang, G.M. Xiao, RSC Adv. 5 (2015) 63697–63704, https://doi.org/10.1039/c5ra07593a.
[15] S. He, H.R. Goldhoorn, Z. Tegudeer, A. Chandel, A. Heeres, M.C.A. Stuart, H.J. Heeres, Submitted (2021).
[16] N.N. Xu, D.H. Pan, Y.F. Wu, S.Q. Xu, L.J. Gao, J. Zhang, G.M. Xiao, React. Kinet., Mech. Catal. 127 (2019) 449–467, https://doi.org/10.1007/s11144-019-01566-0.
[17] F. Wang, X.Z. Chu, P.S. Zhao, F.X. Zhu, Q.Q. Li, F.Y. Wu, G.M. Xiao, Fuel 262 (2020) 1–9, https://doi.org/10.1016/j.fuel.2019.116538.
[18] D.H. Pan, S.Q. Xu, Y.A. Miao, N.N. Xu, H.Z. Wang, X.H. Song, L.J. Gao, G.M. Xiao, Catal. Sci. Technol. 9 (2019) 739–752, https://doi.org/10.1039/c8cy02217h.
[19] S. He, H.R. Goldhoorn, Z. Tegudeer, A. Chandel, A. Heeres, C. Liu, E. Pidko, H. J. Heeres, Fuel Process. Technol. 221 (2021) 1–12, https://doi.org/10.1016/j.fuproc.2021.106944.
[20] F. Wang, X. Kang, M.X. Zhou, X.H. Yang, L.J. Gao, G.M. Xiao, Appl. Catal., A 539 (2017) 80–89, https://doi.org/10.1016/j.apcata.2017.04.005.
[21] Micromeretics, Model # 251, Ar@87-Zeolites, H-form, NLDFT, Micromeretics, USA, 2017.
[22] A. Shahnazari, Catalytic co-conversion of glycerol and proton-donor species to gasoline-range aromatics over alumina, The University of New Brunswick, 1–113, 2016. ⟨https://unbscholar.lib.unb.ca/islandora/object/unbscholar%3A8006⟩ (accessed on 18 April, 2021).
[23] O. Solcova, L. Matejova, P. Topka, Z. Musilova, P. Schneider, J. Porous Mater. 18 (2011) 557–565, https://doi.org/10.1007/s10934-010-9409-x.
[24] K.S.W. Sing, D.H. Everett, R.A.W. Haul, L. Moscou, R.A. Pierotti, J. Rouquerol, T. Siemieniewska, Pure Appl. Chem. 57 (1985) 603–619, https://doi.org/10.1351/pac198254112201.
[25] F. Hu, X. Wu, Y.M. Wang, X.Y. Lai, RSC Adv. 5 (2015) 54053–54058, https://doi.org/10.1039/c5ra08315j.
[26] D. Li, Y. Chen, J. Hu, B. Deng, X. Cheng, Y. Zhang, Appl. Catal., B 270 (2020) 1–11, https://doi.org/10.1016/j.apcatb.2020.118881.
[27] L.P. Wu, X.J. Li, Z.H. Yuan, Y. Chen, Bull. Korean Chem. Soc. 35 (2014) 525–530, https://doi.org/10.5012/bkcs.2014.35.2.525.
[28] P.F. Corregidor, D.E. Acosta, H.A. Destefanis, Sci. Adv. Mater. 6 (2014) 1203–1214, https://doi.org/10.1166/sam.2014.1894.
[29] J.C. Groen, L.A.A. Peffer, J. Perez-Ramirez, Microporous Mesoporous Mater. 60 (2003) 1–17, https://doi.org/10.1016/s1387-1811(03)00339-1.
[30] G.T. Whiting, F. Meirer, M.M. Mertens, A.J. Bons, B.M. Weiss, P.A. Stevens, E. de Smit, B.M. Weckhuysen, Chemcatchem 7 (2015) 1312–1321, https://doi.org/10.1002/cctc.201402897.
[31] A. Sapi, U. Kashaboina, K.B. Abrahamne, J.F. Gomez-Perez, I. Szenti, G. Halasi, J. Kiss, B. Nagy, T. Varga, A. Kukovecz, Z. Konya, Front. Mater. 6 (2019) 1–12, https://doi.org/10.3389/fmats.2019.00127.
[32] M.M.J. Treacy, J.B. Higgins. MFI - ZSM-5, Calcined, Collection of Simulated xrd Powder Patterns for Zeolites, (Fifth edition).,, Elsevier Science B.V, Amsterdam, 2007, pp. 278–279, https://doi.org/10.1016/B978-044453067-7/50604-3.
[33] B.A. Rezende, A. dos Santos, M.A. Camara, D.J. do Carmo, M. Houmard, A. R. Rodrigues, J.C.C. Rubio, Coatings 9 (2019) 1–12, https://doi.org/10.3390/coatings9110755.
[34] J.R. Scheibler, E.R.F. Santos, A.S. Barbosa, M.G.F. Rodrigues, Desalin. Water Treat. 56 (2015) 3561–3567, https://doi.org/10.1080/19443994.2014.986536.
[35] A.S. Al-Dughaither, H. de Lasa, Ind. Eng. Chem. Res. 53 (2014) 15303–15316, https://doi.org/10.1021/ie4039532.
[36] C. Engtrakul, C. Mukarakate, A.K. Starace, K.A. Magrini, A.K. Rogers, M.M. Yung, Catal. Today 269 (2016) 175–181, https://doi.org/10.1016/j.cattod.2015.10.032.
[37] A.A. Zhokh, A.I. Trypolskyi, P.E. Strizhak, Theor. Exp. Chem. 53 (2017) 276–282, https://doi.org/10.1007/s11237-017-9526-6.
[38] M.I. Zaki, M.A. Hasan, F.A. Al-Sagheer, L. Pasupulety, Colloids Surf., A 190 (2001) 261–274, https://doi.org/10.1016/s0927-7757(01)00690-2.
[39] S.P. Verkleij, G.T. Whiting, D. Pieper, S.P. Esclapez, S.W. Li, M.M. Mertens, M. Janssen, A.J. Bons, M. Burgers, B.M. Weckhuysen, Chemcatchem 11 (2019) 4788–4796, https://doi.org/10.1002/cctc.201900777.
[40] L. Samain, A. Jaworski, M. Edén, D.M. Ladd, D.-K. Seo, F. Javier Garcia-Garcia, U. Häussermann, J. Solid State Chem. 217 (2014) 1–8, https://doi.org/10.1016/j.jssc.2014.05.004.
[41] L. Rodríguez-González, F. Hermes, M. Bertmer, E. Rodríguez-Castellón, A. Jiménez-López, U. Simon, Appl. Catal., A 328 (2007) 174–182, https://doi.org/10.1016/j.apcata.2007.06.003.
[42] K. Ramesh, C. Jie, Y.F. Han, A. Borgna, Ind. Eng. Chem. Res. 49 (2010) 4080–4090, https://doi.org/10.1021/ie901666f.
[43] M. Magomedova, E. Galanova, I. Davidov, M. Afokin, A. Maximov, Catalysts 9 (2019) 1–19, https://doi.org/10.3390/catal9050485.
[44] Z.W. Yu, S.H. Li, Q. Wang, A.M. Zheng, X. Jun, L. Chen, F. Deng, J. Phys. Chem. C 115 (2011) 22320–22327, https://doi.org/10.1021/jp203923z.
[45] N.L. Michels, S. Mitchell, J. Perez-Ramirez, ACS Catal. 4 (2014) 2409–2417, https://doi.org/10.1021/cs500353b.
[46] S. Mitchell, N.L. Michels, J. Perez-Ramirez, Chem. Soc. Rev. 42 (2013) 6094–6112, https://doi.org/10.1039/c3cs60076a.
[47] F. Bauer, H.G. Karge, Characterization of coke on zeolites, in: H.G. Karge, J. Weitkamp (Eds.), Molecular Sieves Volume 5: Characterization II, Springer-Verlag, Berlin and Heidelberg, 2007, pp. 249–364, https://doi.org/10.1007/3829_005.
[48] Y. Ono, Catal. Rev.: Sci. Eng. 34 (1992) 179–226, https://doi.org/10.1080/01614949208020306.
[49] C. Wang, L. Zhang, X. Huang, Y. Zhu, G. Li, Q. Gu, J. Chen, L. Ma, X. Li, Q. He, J. Xu, Q. Sun, C. Song, M. Peng, J. Sun, D. Ma, Nat. Commun. 10 (2019) 4348, https://doi.org/10.1038/s41467-019-12285-4.
[50] D.P. Serrano, R.A. Garcia, M. Linares, B. Gil, Catal. Today 179 (2012) 91–101, https://doi.org/10.1016/j.cattod.2011.06.029.
[51] A. Errekatxo, A. Ibarra, A. Gutierrez, J. Bilbao, J.M. Arandes, P. Castano, Chem. Eng. J. 307 (2017) 955–965, https://doi.org/10.1016/j.cej.2016.08.100.
[52] B. Liu, D. Slocombe, M. AlKinany, H. AlMegren, J. Wang, J. Arden, A. Vai, S. Gonzalez-Cortes, T. Xiao, V. Kuznetsov, P.P. Edwards, Appl. Petrochem. Res. 6 (2016) 209–215, https://doi.org/10.1007/s13203-016-0156-z.